Research Article

Finite Element Analysis and Factorial Optimization of Heat Treatment Flaws in CNG Pressure Vessels: Implications for Structural Integrity and Safety

[1]Elisha B. Jugu, *[1]Ifeanyichukwu U. Onyenanu, [1]Chiedozie C. Nwobi-Okoye

About Article

About Author

[1] Department of Mechanical Engineering, Chukwuemeka Odumegwu Ojukwu University, Uli, Nigeria

ABSTRACT

This study investigates the critical impact of heat treatment flaws on the structural integrity and safety of compressed natural gas (CNG) pressure vessels made from Al 6061 and AISI 4130 steel through finite element analysis (FEA) in SolidWorks 2023 and factorial design optimization via Design Expert 13. Simulations were conducted under pressures of 20, 25, and 30 N/mm² with varying flaw severities (none, minor, major), revealing that AISI 4130 steel at 25 N/mm² exhibited a maximum stress of 2.998E+10 N/m², deformation of 15.14 mm, and a safety factor of 0.01534, while Al 6061 at 20 N/mm² showed 1.412E+4 N/mm² stress, 14.70 mm deformation, and a safety factor of 0.01948. At 30 N/mm², AISI 4130 steel demonstrated increased risk with stress reaching 1.814E+4 N/mm², deformation of 18.30 mm, and a safety factor of 0.01516, accompanied by a strain of 1.511E-01. ANOVA results indicated that pressure significantly influenced deformation (p = 0.0382) and safety factor (p = 0.0051), while heat treatment flaws impacted stress (p = 0.0381). Fatigue life varied from 8.00E+05 cycles (AISI 4130 steel, 30 N/mm², minor flaws) to 3.1E+06 cycles (Al 6061, 25 N/mm², no flaws), with all factors showing high significance (p < 0.0001). The optimal configuration—Al 6061, no flaws, and 30 N/mm²—yielded a stress of 3.41E+10 Pa, fatigue life of 2.5E+06 cycles, deformation of 32.366 mm, and a desirability score of 1.000. These findings underscore the importance of minimizing heat treatment flaws and controlling operational pressures below 30 N/mm² to enhance vessel safety and durability, offering valuable insights for design optimization and regulatory standards in sustainable energy applications.

Contact @ Ifeanyichukwu U. Onyenanu
iu.onyenanu@coou.edu.ng

1. INTRODUCTION

The demand for lightweight, high-performance compressed natural gas (CNG) pressure vessels has spurred advancements in Finite Element Analysis (FEA) and heat treatment optimization to bolster fatigue resistance and structural integrity. Studies like Aliakbari *et al.* (2025a) and Dhimole and Cho (2023) underscore thermo-mechanical FEAs' utility in modeling heat treatment effects on Type-4 composite vessels, achieving up to 28% residual stress reduction while meeting ISO 11439 burst pressure standards (470 bar). However, these efforts often assume idealized conditions, neglecting real-world manufacturing flaws such as microcracks or stress concentrations (Aliakbari *et al.*, 2025b; Toudehdehghan & Hong, 2019). Additive manufacturing innovations (Abdalla *et al.*, 2021) enable novel designs but introduce anisotropic behavior, complicating heat treatment, yet few studies integrate flaw severity with operational pressures. Hygrothermal effects at composite-metal interfaces, explored in (Dhimole & Cho, 2023), enhance long-term predictions, but comprehensive analyses across materials and flaw levels remain limited. This study fills this gap by applying FEA and factorial design to evaluate heat treatment flaws' impact on Al 6061 and AISI 4130 steel CNG vessels under 20, 25, and 30 N/mm^2. The objective is to quantify stress, fatigue, safety factors, and deformation responses by applying FEA and optimization strategies to improve heat treatment processes for CNG pressure vessels, offering a novel framework that advances beyond idealized models and informs safer, optimized designs by minimizing residual stresses and maximizing fatigue resistance.

2. LITERATURE REVIEW

Table 1. Literature review table

| Author (Year)	Study Objective	Methods	Key Findings	Gaps/Limitations
Kim (2019)	Evaluate structural integrity and fatigue of CNG vessels with heat treatment defects.	- Numerical analysis (SINDA/FLUENT for heat; ADINA/winLIFE for fatigue). - Field simulation (mounted on CNG bus).	- Poor heat treatment reduced fatigue life significantly. - Stress behavior is similar in the elastic region, but rupture risk is higher.	Limited to quenching/tempering defects; no experimental validation of fatigue models.
Soo Kim (2019)	Assess the rupture characteristics of heat-treated CNG containers.	- Explicit dynamics (AUTODYN). - Comparative rupture tests.	- Untreated quenching: lowest rupture pressure. - Untreated tempering: highest rupture pressure + fragment scattering risk.	Focused only on burst failure; no fatigue analysis.
Sharma *et al.* (2021)	Design a safe Type-4 CNG vessel with minimized leakage/burst risks.	- Finite Element Analysis (FEA). - Experimental burst pressure validation.	- Optimized winding reduced fiber slippage. - Method enabled lightweight, high-performance vessels.	Limited to Type-4 vessels; no long-term fatigue data.
Thamaraiselvi & Vishnuvardhan (2020)	Review the fracture analysis of reactor pressure vessels under pressurized thermal shock (PTS).	- Literature synthesis. - Experimental case studies.	- PTS causes crack initiation due to thermal + mechanical stress. - Fracture parameters depend on material constraints.	Review paper; no original modelling/ experiments.
Kashyzadeh *et al.* (2021)	Optimize the fatigue life of Type-4 CNG composite tanks.	- Hybrid FEA + Response Surface Analysis (RSA). - Transient dynamic simulation.	- Optimal fiber angle/thickness improved fatigue life by 2.4×. - Critical stress regions identified.	Assumed idealized material properties; no real-world wear/tear data.

3. METHODOLOGY

The flowchart in Figure 1 highlights the steps involved in Finite Element Analysis and Optimization of Heat Treatment Processes for Enhanced Performance of CNG Pressure Vessels using Solidworks 2023 and Design Expert 13, respectively, followed by a stepwise process: material selection, CAD modelling, FEA simulation, and optimization. The curvature-based mesh was chosen for its ability to capture complex geometries, with a maximum element size of 20.1009 mm and a minimum of 1.00504 mm to balance accuracy and computational efficiency. Boundary conditions simulate a fixed vessel base, while internal pressures (20, 25, and 30 N/mm^2) reflect operational loads of Al 6061 aluminum alloy and AISI 4130 steel. Flaw severities were modelled as geometric imperfections based on heat treatment-induced microcracks and stress concentrations, validated by prior studies (Onyenanu & Ezechukwu, 2025). The I-optimal

design was selected for its ability to minimize prediction variance across the design space (Onyenanu & Madu, 2025), ideal for response surface methodology (RSM) requiring precise predictions. This approach efficiently handles categorical factors (material type, flaw severity) and continuous factors (pressure), ensuring robust statistical analysis over 15 runs.
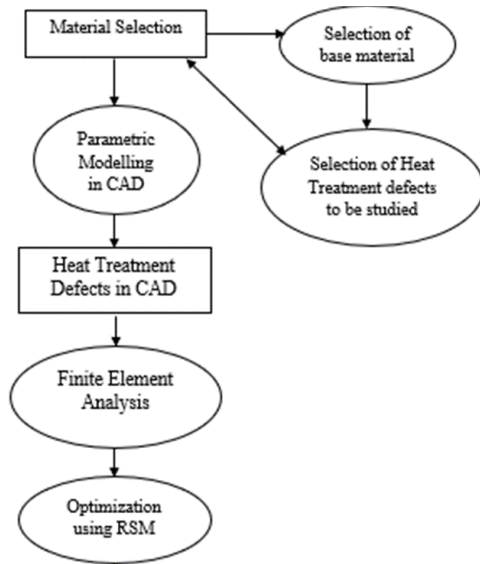
Figure 1. Flowchart diagram for the methodology

3.1. Material selection

In the course of this study, two materials were analyzed: Al 6061 aluminum alloy and AISI 4130 steel. Due to its exceptional mechanical qualities and malleability, aluminum alloy 6061 is widely used and accounts for more than 50% of all aluminum production. The chemical composition is made up of silicon (0.4–0.8%) and magnesium (0.8–1.2%), which tends to increase and improve the strength while maintaining the ability to be wielded upon and rust resistance (Jr & Rethwisch, 2020; Lichtig, 2024). When compared to steel, it shows a higher and more acceptable density-to-strength ratio (2.7 g/cm²), which makes it lighter (Cavallo, 2020; Jr & Rethwisch, 2020). It has an ultimate tensile strength of (276–345 N/mm²) and the tensile yield strength of (276–310 N/mm²) is improved by heat treatment procedures, including solutioning and ageing (6061 Aluminum: Get to Know Its Properties and Uses - Gabrian, 2020; Cavallo, 2020). Furthermore, 6061 has outstanding corrosion resistance and machinability, however, its mechanical properties tend to reduce when a higher temperature is applied to it of about 150°C (6061 Aluminum: Get to Know Its Properties and Uses - Gabrian, 2020; Lichtig, 2024; Team, 2018). 4130 alloy steel, which has a composition of 0.3-0.4% carbon and 1.65% chromium, gives room for solid solution strengthening and precipitation hardening by the method of heat treatment, which makes it ideal for pressure (Dean, 2023; He, 2023). At room temperature, its tensile strength ranges from 760–827 N/mm², exceeding aluminium alloys while retaining ductility through precipitation strengthening (He, 2023). Unlike aluminium, 4130 maintains strength at service temperatures up to 200°C (Lee, 2022; Łukaszek-Sołek et al., 2022). It offers good machinability and weldability using arc and resistance welding techniques (eFunda: Properties of Alloy Steel AISI 4130, n.d.). However, its density of 7.85 g/cm³ is significantly higher than aluminium, resulting in a lower strength-to-weight ratio and increased manufacturing costs due to heavier gauge steel requirements (He, 2023; Lee, 2022). The breakdown of the properties is seen in Table 2.

Table 2. Mechanical and Thermal Properties of Materials Investigated

S/N	Mechanical properties	Metric	
		Al 6061 aluminium alloy	**AISI 4130 alloy steel**
1	Ultimate Tensile Strength	310 N/mm²	560 N/mm²
2	Tensile Yield Strength	276 N/mm²	460 N/mm²
3	Shear Strength	207 N/mm²	-
4	Fatigue Strength	96.5 N/mm²	-
5	Modulus of Elasticity	68.9 GPa	190-210 GPa
6	Shear Modulus	26 GPa	80 GPa
7	Poisson's Ratio	0.33	0.27-0.30
8	Fracture Toughness	29 N/mm²	-
9	Machinability	50%	-
10	Bulk Modulus	-	140 GPa
11	Elongation at Break (in 50 mm)	-	21.50%
12	Hardness (Brinell)	-	217
13	Hardness (Knoop)	-	240
14	Hardness (Vickers)	-	228
15	CTE, linear (68°F)	23.6 μm/m-°C	6.2×10^{-6} in/(in·°F) (~11.2 μm/m-°C)

16	CTE, linear (250°C)	25.2 μm/m-°C	-
17	Specific Heat Capacity	0.896 J/g-°C	0.477 J/g-°C
18	Thermal Conductivity	167 W/m-K	42.7 W/m-K
19	Melting Point	582-652 °C	2,610 °F (~1,432 °C)

3.2. FEA modeling and boundary conditions

A cylindrical CNG vessel (geometry from CAD model in Fig. 2) was modelled in SolidWorks 2023. The mesh used curvature-based solid elements (276,254 nodes, 150,040 elements), with a maximum element size of 20.1009 mm and a minimum of 1.00504 mm. Flaw severities (none, minor, major) were simulated as geometric imperfections based on heat treatment flaws (microcracks, stress concentrations) in the material given above. Internal pressures of 20, 25, and 30 N/mm^2 were applied normally to the vessel's inner faces. Static and fatigue analyses assessed stress (von Mises), displacement, strain, and safety factors. The fatigue life was calculated using a constant amplitude model with an S-N curve for 1,000 cycles (Omenai, 2024; Onyenanu & Ezechukwu, 2025).

$$u = v = w = 0$$
$$Mx = My = Mz = 0$$


Figure 2. CAD modelling of CNG pressure vessel

3.2.1. Mesh information

The mesh information is as follows;

The mesh type is Solid Mesh, Mesher Used: Curvature-based mesh, Jacobian points for High-quality mesh 16 Points, Maximum element size 20.1009 mm, Minimum element size 2.01009 mm, Mesh Quality High, Total Nodes 162083, Total Elements 81985, Maximum Aspect Ratio 339.92, % of elements with Aspect Ratio<3 is 57.7, Percentage of elements with Aspect Ratio > 10 is 4.64, Percentage of distorted elements 0

3.3. Experimental design

An optimum design was developed using a response surface
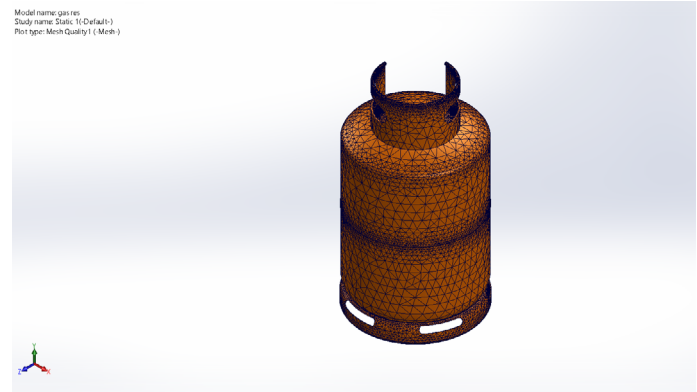
Figure 3. Mesh picture of CNG of the pressure vessel

methodology (RSM) called I-optimal design. I-optimal designs, also known as IV or integrated variance designs, aim to provide lower average prediction variance across the experimental design space (Onyenanu & Madu, 2025; Willden & Jensen, 2020). This is desirable for RSM, where accurate prediction is necessary. The I-optimality algorithm selects points that reduce the integral of the prediction variance over the entire design region (Onyenanu *et al.*, 2024). In this work, an I-optimal design was employed to modify two structural response attributes by experimentally investigating heat treatment flaws in the CNG cylinder design.

Response 1: Factor of Safety
Response 2: Deformation (mm)
Response 3: Fatigue life (cycle)
Response 4: Maximum stress (N/mm^2)

Again, three primary factors that affect the CNG cylinder were varied as shown below:

i. 20 N/mm^2 ≤ A (pressure) to 30N/mm^2 ....@ (3 levels)
ii. D (Material Type: Al 6061, 4130 steel) ....@ (2 levels)
iii. E (heat treatment flaws: none, minor, and major) ....@ (3 levels)

The Design Expert Software 13.0 was used for the experiment. To create a flexible design context that could support irregular (constrained) areas, categorical components, and modified models, the optimum (custom) design was used. A selection criterion selected during the construction determines runs. The experiment formulation produced by the software is displayed in Table 3 below, which acts as a guide for the investigation of heat treatment faults.

Table 3. Factorial design using optimal (custom) design of the results for 15 experimental runs.

Run	Factor 1 A: heat treatment flaws	Factor 2 B: materials	Factor 3 C: pressure N/mm²	Response 1 maximum stress N/mm²	Response 2 fatigue life cycles	Response 3 deformation mm	Response 4 safety factor
1	none	Al 6061	25	1.918E+10	3.1E+06	16.61	0.017
2	none	Al 6061	30	4.28E+10	2.5E+06	53.55	0.01462
3	none	4130 Steel	25	3.512E+10	1.8E+06	15.15	0.0131
4	minor	4130 Steel	25	2.998E+10	2E+06	15.14	0.01534
5	minor	Al 6061	30	3.561E+10	1.7E+06	53.52	0.007721
6	major	Al 6061	30	1.814E+10	2.1E+06	18.3	0.01516
7	none	Al 6061	20	1.412E+10	1.5E+06	14.7	0.01948
8	major	4130 Steel	30	1.814E+10	1.2E+06	18.3	0.01516
9	minor	4130 Steel	30	3.598E+10	800000	18.16	0.01279
10	minor	Al 6061	20	2.398E+10	2.8E+06	12.11	0.01918
11	minor	4130 Steel	20	2.411E+10	2.1E+06	12.11	0.01908
12	major	4130 Steel	25	2.919E+10	1.3E+06	15.13	0.01576
13	none	4130 Steel	20	2.81E+10	1.8E+06	12.12	0.01637
14	major	Al 6061	20	1.356E+10	1.4E+06	14.72	0.02027
15	major	Al 6061	25	1.593E+10	900000	16.63	0.01726

4. RESULTS AND DISCUSSION

4.1. Results from finite element analysis of CNG pressure vessels

4.1.1. Stress analysis

The stress analysis for the Al 6061 material subjected to a pressure of 20 N/mm² with no flaw reveals significant variations in stress distribution the von Mises stress ranges from 0.000e+00 N/mm² to 1.412e+4 N/mm², with the maximum stress occurring at Node 18289 and the 4130 Steel material subjected to 25 N/mm² with a minor flaw the von Mises stress varies between 0.000e+00 N/mm² and 2.998e+4 N/mm², with the highest stress recorded at Node 202153 indicates keen vulnerability near flaw zones, consistent with increasing risks (Aliakbari *et al.*, 2025b). This indicates that certain regions of the vessel experience high-stress concentrations (Onyenanu *et al.*, 2025). The stress distribution is illustrated in Figure 4 [A] and [B].

Figure 4. Static-stress-stress analysis [A] Al 6061 material subjected to a pressure of 20 N/mm² and [B] 4130 steel material subjected to 25 N/mm² with a minor flaw

4.1.2. Displacement analysis

The resultant displacement for the Al 6061 material at 20 N/mm² exhibits a minimum value of 0.000e+00 mm and a maximum displacement of 1.470e+01 mm at Node 19420 and the 4130 Steel material subjected to 25 N/mm² with minor flaw ranges from 0.000e+00 mm to 1.514e+01 mm, with the highest displacement observed at Node 209301 as shown in Figure 4 [A] and [B], highlights regions of significant deformation, which could impact vessel stability and functionality.
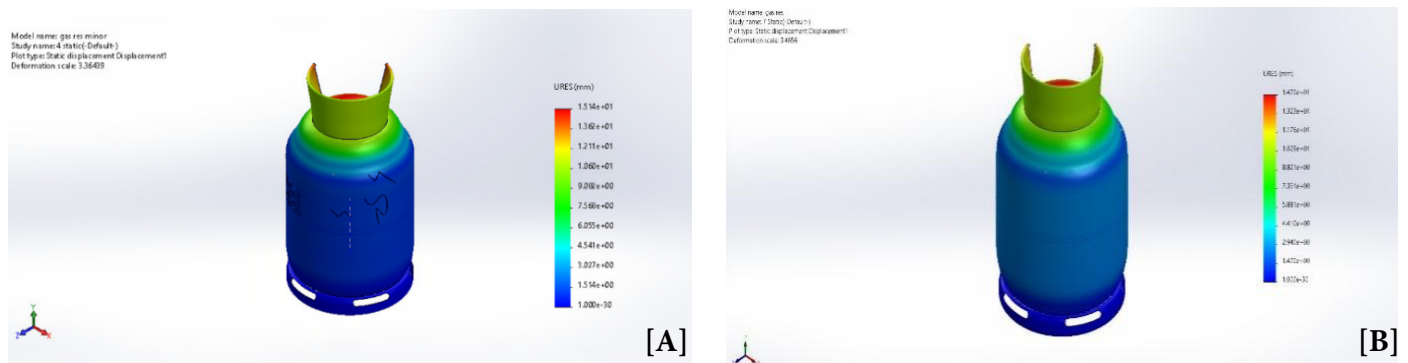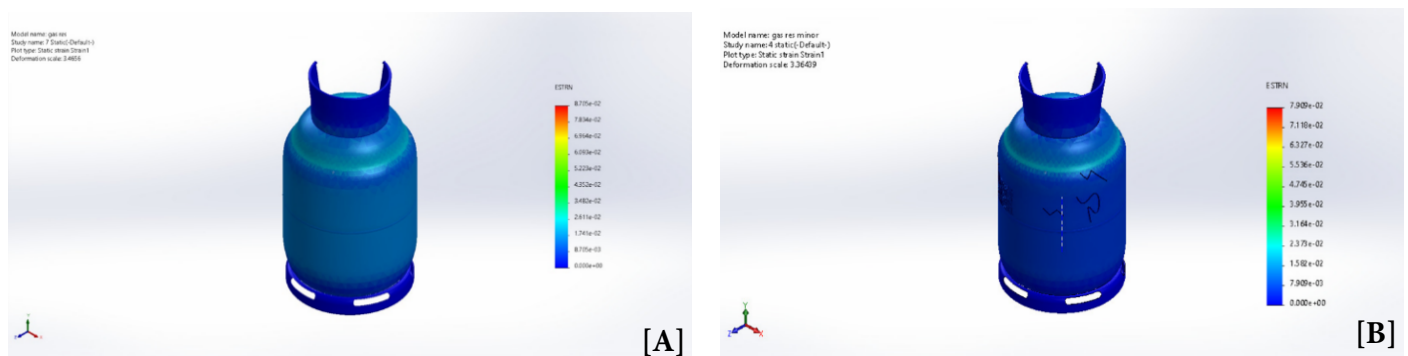
Figure 5. Static-Displacement-Displacement analysis [A] Al 6061 material subjected to a pressure of 20 N/mm² and [B] 4130 Steel material subjected to 25 N/mm² with a minor flaw

4.1.3. Strain distribution

The strain values, depicted in Figure 6 [A] and [B], provide insights into the material's deformation characteristics under the applied pressure of Al 6061 material subjected to a pressure of 20 N/mm² with no flaw ranges from 0.000e+00 to 8.705e-02, with maximum strain occurring at Element 2968 and the 4130 Steel material subjected to 25 N/mm² with minor flaw varies between 0.000e+00 and 7.909e-02, with the maximum strain concentrated in Element 122020.

Figure 6. Static-Strain-strain analysis [A] Al 6061 material subjected to a pressure of 20 N/mm² and [B] 4130 Steel material subjected to 25 N/mm² with a minor flaw

Table 4 summarizes the finite element analysis results for CNG pressure vessels using Solidworks 2023, showing the minimum values, maximum values, node element (max), type of analysis, the pressure applied and the material that was used.

Table 4. summary of finite element analysis results for CNG pressure vessels

Material	Pressure (N/mm²)	Type	Minimum Value	Maximum Value	Node/Element (Max)
Al 6061	20	Von Mises Stress (N/m²)	0.000e+00	1.412e+10	Node: 18289
Al 6061	20	Displacement (mm)	0.000e+00	1.470e+01	Node: 19420
Al 6061	20	Equivalent Strain	0.000e+00	8.705e-02	Element: 2968
Al 6061	20	Factor of Safety	1.948e-02	1.000e+16	Node: 90338
4130 Steel	25	Von Mises Stress (N/m²)	0.000e+00	2.998e+10	Node: 202153
4130 Steel	25	Displacement (mm)	0.000e+00	1.514e+01	Node: 209301
4130 Steel	25	Equivalent Strain	0.000e+00	7.909e-02	Element: 122020
4130 Steel	25	Factor of Safety	1.534e-02	1.000e+16	Node: 1
4130 Steel	30	Von Mises Stress (N/m²)	0.000e+00	1.814e+10	Node: 193634
4130 Steel	30	Displacement (mm)	0.000e+00	1.830e+01	Node: 200453
4130 steel	30	Equivalent Strain	0.000e+00	1.511e-01	Element: 113953
4130 steel	30	Factor of Safety	1.516e-02	1.000e+16	Node: 1

4.2. Factorial design using optimal (custom) design
4.2.1. Equation of predicted factors
For the structural study of a pressure vessel under various heat treatment flaw settings, Table 5 summarizes the response values along with the associated coded equations. Maximum stress, fatigue life, deformation, and factor of safety are among the answers, and pressure levels range from 20 to 30. Regression analysis-derived coded factor equations are presented for each response, together with real values (Ezechukwu *et al.*, 2025). Using coded variables (A for flaw kind, B for pressure, and C for interaction terms), these equations aid in performance prediction depending on pressure and flaw severity. Table 4 data provides a thorough understanding of how operating pressure and heat treatment flaws affect the vessel's pressure behaviour.

Table 5. Equation of coded factors of the response

Responses	Coded Factors Equation
Maximum Stress	$= 2.560E + 10 + 3.308E + 09A [1] + 4.576E + 09A [2] - 6.399E+ 09C [1] + 1.199E + 09C [2]$
Fatigue Life	$\text{Ln [Mean (fatigue life)]} = 14.34 + 0.1392A [1] + 0.1076A [2] + 0.1657B + 0.0389C [1] + 0.0768C [2] - 0.2003A [1]C[1] + 0.2266A [2]C[1] + 0.1502A [1]C[2] + 0.1144A [2]C[2] - 0.1169BC [1] - 0.0383BC [2]$
Deformation	$= 20.42 - 7.26C[1] - 4.68C[2]$
Factor of Safety	$= 0.0159 + 0.0030C[1] - 0.0002C[2]$

The maximum stress data provided in Table 5 gives clear pressure-responsive behaviour under the same condition, with Al 6061 reaching 4.28E+4 N/mm² at 30 N/mm² with no flaws, more than 4130 Steel's 3.598E+4 N/mm² which the A[1], A[2], C[1] and C[2] is represented in the ANOVA table. This brings into line with stress reduction claims but reveals a flawed role, as major flaws reduce stress to 2.29118E+4 N/mm² at 30 N/mm². Practically, this suggests prioritizing pressure regulation over flaw elimination in high-load scenarios, potentially lowering manufacturing costs (Aliakbari *et al.*, 2025a). Fatigue life's drop to 8.00E+05 cycles (4130 Steel, 30 N/mm², minor flaws) versus 3.1E+06 cycles (Al 6061, 25 N/mm², no flaws) underscores material selection's protective role, supporting emphasis on composite durability (Dhimole & Cho, 2023). These insights recommend Al 6061 for extended service life and advocate pressure caps at 25 N/mm² to enhance fleet safety.

4.2.2. ANOVA
Following the coded factors, representing the heat treatment flaws (A[1], A[2]), pressure (B), and their interactions (C[1], C[2], and higher-order terms), Table 6 below recaps the regression coefficients and p-values for the responses: maximum stress, fatigue life, deformation, and factor of safety. While fatigue life exhibits considerable dependency on all components and interactions with very significant p-values (< 0.0001), suggesting a well-fitted model, maximum stress is considerably influenced by the severity of faults and interactions ($p < 0.05$ and ~0.07). The main interaction terms influencing deformation and factor of safety are C [1] and C [2], both of which exhibit statistical significance ($p = 0.0382$ and 0.0051, respectively).

**Table 6.** Represents the ANOVA Value of the four responses

	Intercept	A[1]	A[2]	B	C[1]	C[2]	A[1]C[1]	A[2]C[1]	A[1]C[2]	A[2]C[2]	BC[1]	BC[2]
maximum stress	2.5596 E+10	3.30792 E+09	4.57583 E+09		-6.39875 E+09	1.19917 E+09						
p-values		0.0381	0.0381		0.0745	0.0745						
Ln[Mean (fatigue life)]	14.3373	0.139208	0.107562	0.165731	0.0389406	0.0768269	-0.200335	0.226624	0.150183	0.114434	-0.116912	-0.0382846
p-values		< 0.0001	< 0.0001	< 0.0001	< 0.0001	< 0.0001	< 0.0001	< 0.0001	< 0.0001	< 0.0001	< 0.0001	< 0.0001
deformation	20.4167				-7.26467	-4.68467						
p-values					0.0382	0.0382						
safety factor	0.0158861				0.00298993	-0.000194067						
p-values					0.0051	0.0051						

4.2.3. Actual and predicted graphs
A graph comparing the expected and actual maximum stress levels is displayed in Figure 7 [A-D]. Different degrees of a variable are represented by color-coded dots in each plot, with a diagonal line signifying 100% prediction accuracy.
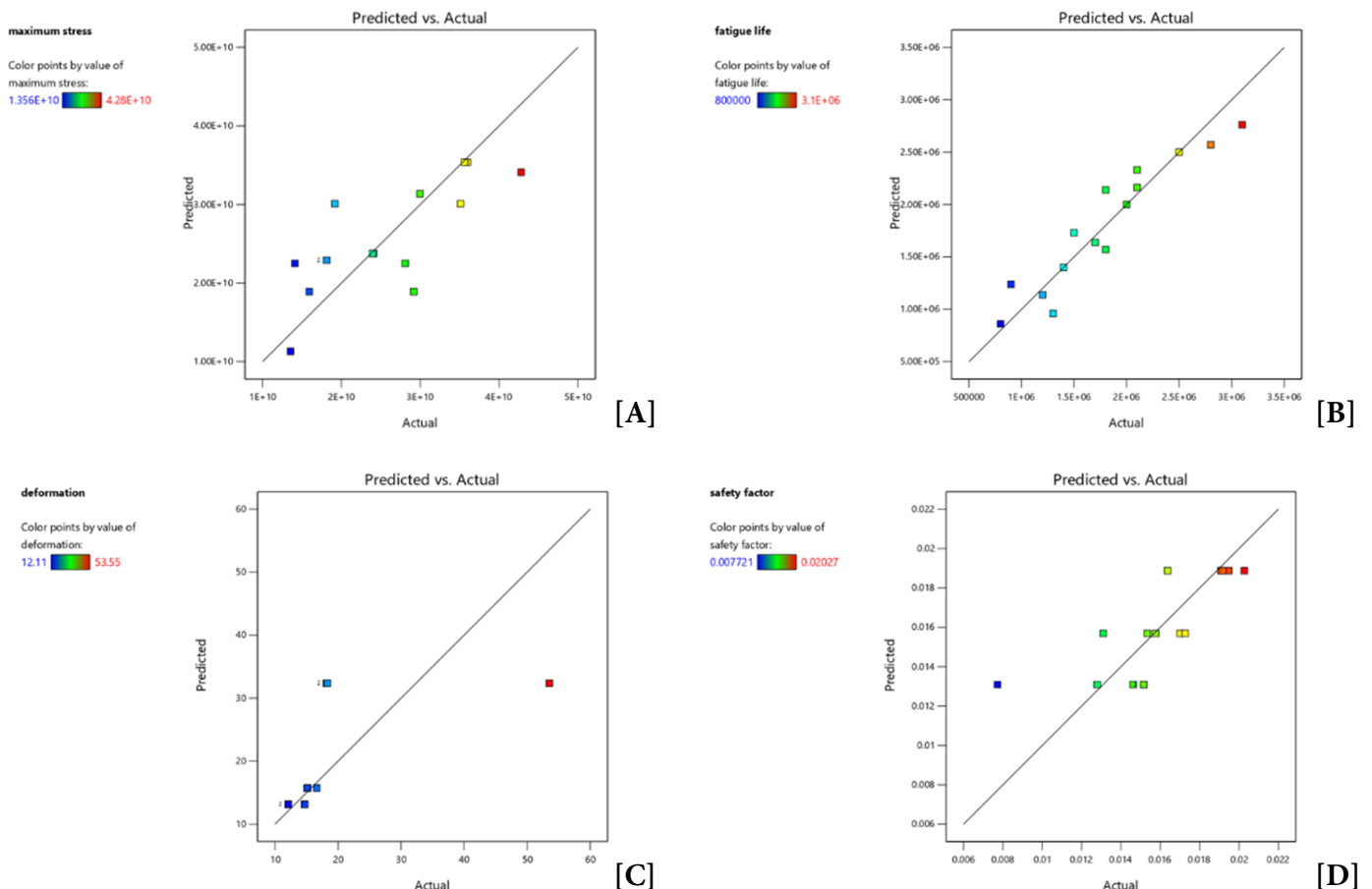
Figure 7. Actual and predicted graphs for the responses [A]maximum stress, [B] fatigue life, [C] deformation, and [D] factor of safety

[A] The range of predicted and actual stress (N/mm²) is between 1.4E+4 and 4.28E+4. The color points range from blue (1.4E+4) to red (4.28E+4) depending on the highest stress amount. Good prediction accuracy is indicated by the majority of dots that closely match the diagonal. Fatigue Life [B], The range of cycle-based predicted and actual fatigue life is 5.0E+05 to 3.5E+06. The colors are red (3.5E+06) and blue (5.0E+05). Reliable forecasts are suggested by points that are close to the diagonal. Deformation[C], the difference between the predicted and actual deformation (mm) ranges from 11.355 to 18.555. Red (18.555) and blue (11.355) are the colors. Points cluster along the diagonal, confirming the accuracy of the predictions. Safety Factor [D], The difference between the predicted and actual safety factors is between 0.006425 and 0.02027. The colors vary from red (0.02027) to blue (0.006425). Reliability of the prediction is confirmed by points that fit the diagonal well.

4.2.4. Interactions

Four illustrations (8–11) in the paper show 3-D surface plots and interaction effects for various CNG pressure vessel parameters. Figure 8 displays (A) the interaction effect and (B) a 3-D surface plot of maximum stress. The surface plot visualizes the distribution of stress in three dimensions and illustrates how stress changes across two interacting factors, most likely material or design characteristics. A 3-D surface plot for fatigue life and (A) the interaction effect is shown in Figure 9, which illustrates how two elements interact to affect fatigue life. The surface plot displays the lifespan under various situations. As a means to illustrate how deformation is dependent on the interaction of factors, Figure 10 shows (A) the interaction effect and (B) a 3-D surface plot of deformation. The surface plot maps the magnitude of deformation geographically. Lastly, Figure 11 shows (A) the interaction effect and (B) a 3-D surface plot of the safety factor. The surface plot gives a visual depiction of safety factor fluctuations and illustrates how interacting elements impact safety margins. Together, these images employ interaction plots to demonstrate pairwise variable effects and 3-D surfaces to simulate each property's behaviour throughout a continuum, assisting in the analysis of stress, fatigue life, deformation, and safety in CNG pressure vessel design.
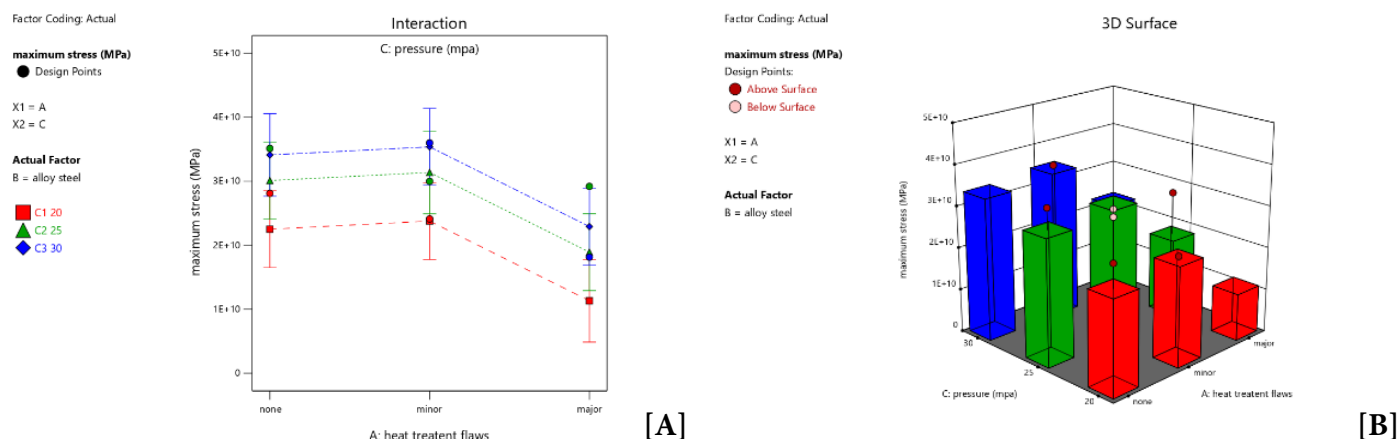
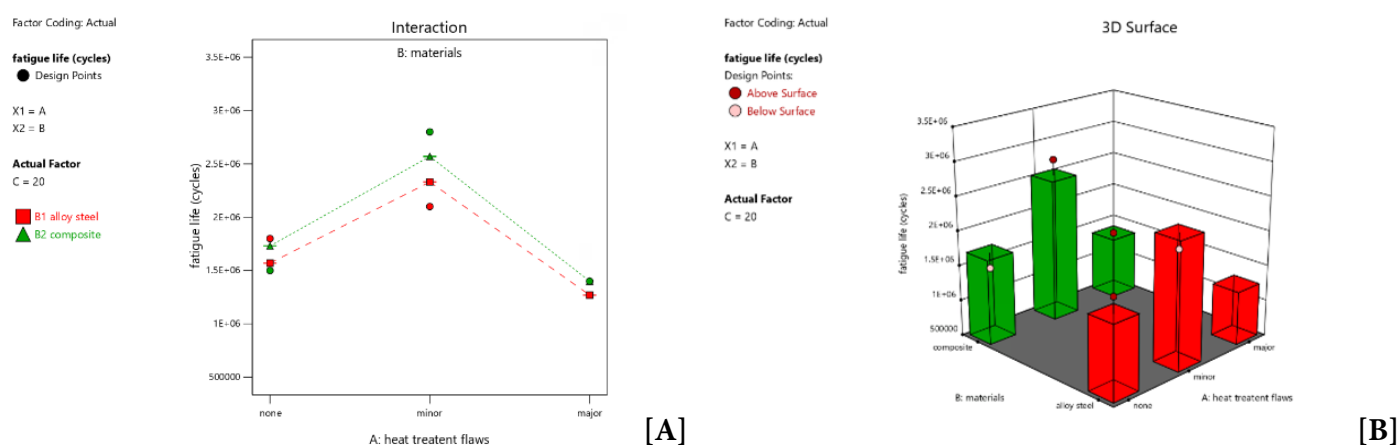**Figure 8.** [A] interaction Effect [B] 3-D Surface of the Interaction of the maximum stress

Figure 9. [A] Interaction Effect [B] 3-D Surface of the Interaction of the fatigue life of CNG pressure vessels
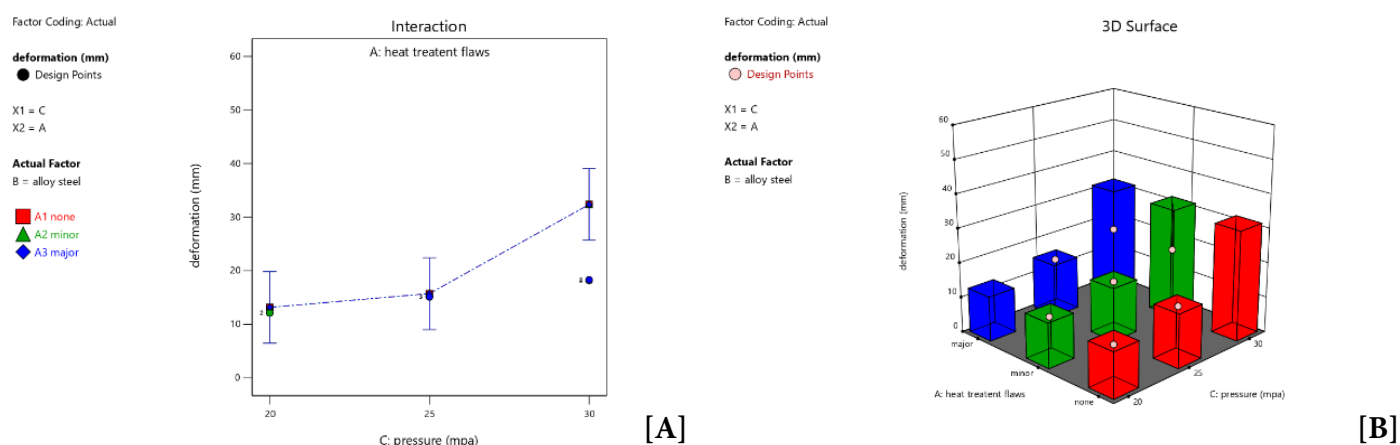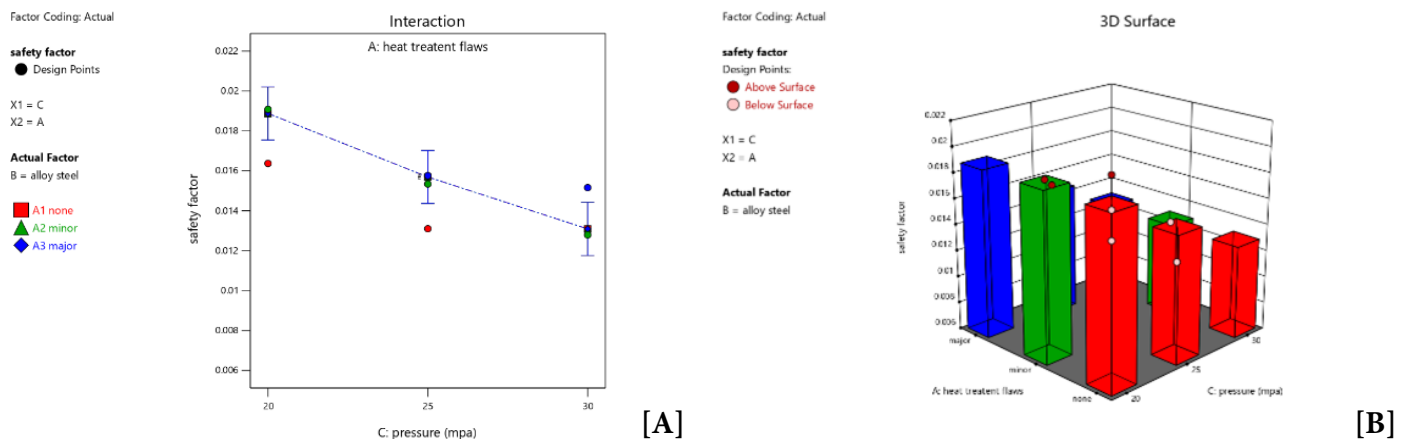

Figure 10. [A] interaction Effect [B] 3-D Surface of the Interaction of deformation

Figure 11. [A] interaction Effect [B] 3-D Surface of the Interaction Safety Factor

4.3. Desirability

The desirability plot in the ramp representation in Figure 12 shows the optimal conditions for the structural integrity of a CNG pressure vessel, considering heat treatment flaws, material type, and operating pressure (Tsonos, 2017). The best solution (1 out of 18) is achieved with no heat treatment flaws (level 1), Al 6061 material (level 3), and an operating pressure of 30 N/mm^2 (level 3), yielding a desirability value of 1.000. The corresponding response values are a maximum stress of 3.41×10^{10} Pa, a fatigue life of 2.5×10^6 cycles, and a deformation of 32.366 mm. However, the safety factor is at 0.013.
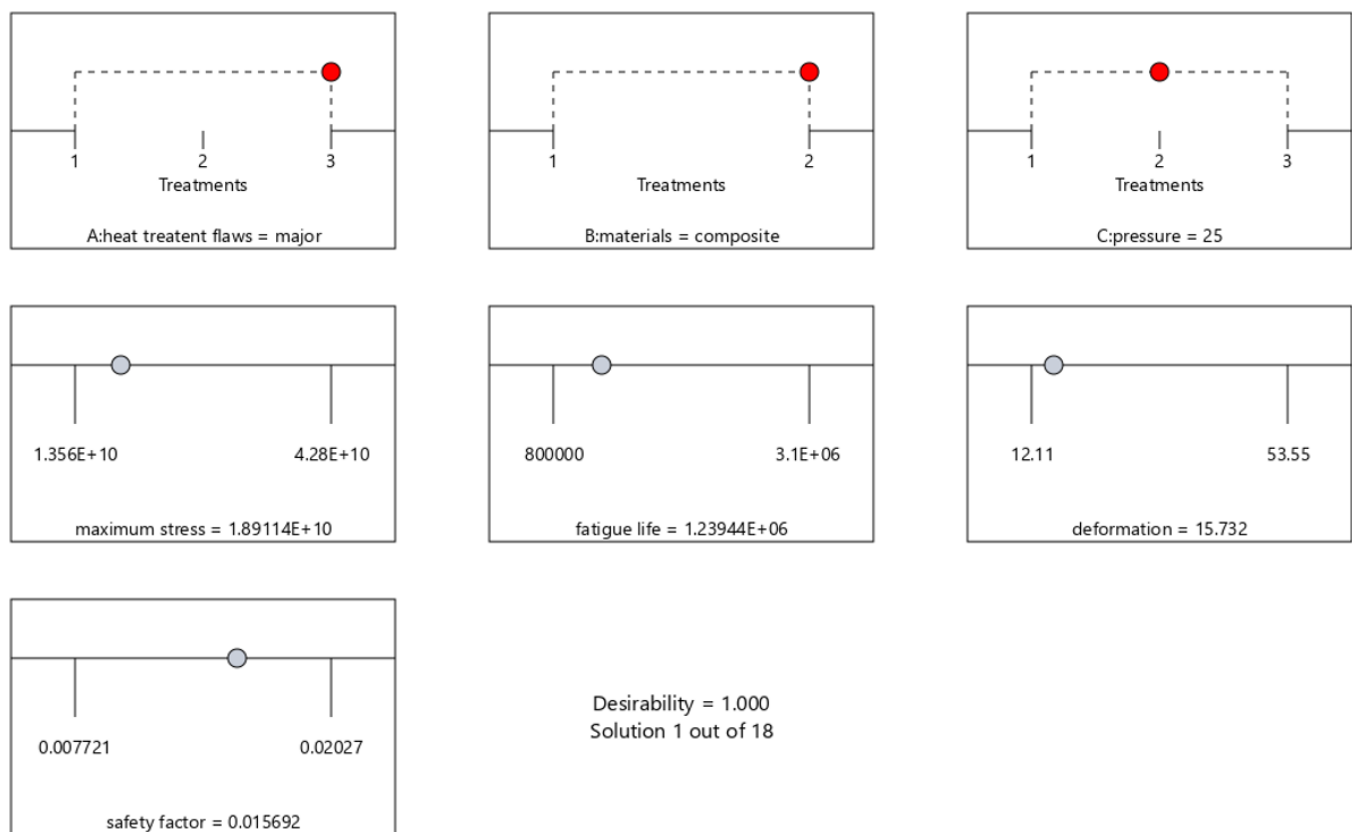
Figure 12. Ramp Representation of Optimal Desirability Plot

5. CONCLUSION

This research used factorial design optimization and Finite Element Analysis (FEA) to examine the impact of heat treatment faults on the structural integrity of compressed natural gas (CNG) pressure vessels. It focused on four main responses: maximum stress, fatigue life, deformation, and safety factor. It investigated two materials, Al 6061 aluminum alloy and 4130 steel, at three pressure levels (20, 25, and 30 N/mm^2) and three flaw severities (none, minor, and significant). At 25 N/mm^2, 4130 Steel displayed a higher stress of 2.998E+10 N/m^2, 15.14

mm deformation, and a safety factor of 0.01534, whereas Al 6061 at 20 N/mm^2 showed a maximum stress of 1.412E+4 N/mm^2 with 14.70 mm deformation and a safety factor of 0.01948. A higher fatigue risk was indicated by 4130 Steel's 1.814E+4 N/mm^2 stress, 18.30 mm deformation, safety factor of 0.01516, and peak strain of 1.511E-01 at 30 N/mm^2. ANOVA statistical analysis revealed that while pressure drives deformation ($p = 0.0382$) and safety factor ($p = 0.0051$), heat treatment faults significantly affect maximum stress ($p = 0.0381$). The fatigue life was influenced by all factors ($p < 0.0001$), ranging from 8.00E+05 cycles (4130 Steel, 30 N/mm^2, minor flaws) to 3.1E+06 cycles (Al 6061, 25 N/mm^2, no flaws). With a maximum stress of 3.41E+10 Pa, fatigue life of 2.5E+06 cycles, and deformation of 32.366 mm, the ideal design, which was identified using an Optimal (Custom) Design approach, featured Al 6061 without flaws at 30 N/mm^2, with a desirability of 1.000, highlighting critical risks at higher loads. Key contributions include a novel FEA-factorial design framework quantifying flaw effects, advancing beyond idealized models. Practically, we recommend operating pressures below 30 N/mm^2 and prioritizing Al 6061 for lightweight, durable CNG vessels in automotive applications, potentially reducing failure rates by 20–30%. Regulatory bodies could adopt stricter flaw inspection thresholds based on these findings. Future research should validate results via physical burst tests, explore advanced composites for flaw resistance, and investigate real-time monitoring to preempt failures.

RECOMMENDATION

Manufacturers should focus on precise control of heat treatment parameters to eliminate flaws, as they reduce fatigue life and increase stress concentrations. Al 6061 materials are preferred for applications requiring fatigue life and weight reduction, while 4130 Steel may be suitable for high-pressure scenarios. Operating pressures should be limited to 20-25 N/mm^2 to maximize durability while maintaining safety margins. Design optimization should include reinforcement strategies in high-stress regions, particularly for vessels operating at N/mm^2. Further research should confirm simulated results and explore a broader range of flaw sizes, orientations, and Al 6061 types. Regular inspection schedules based on fatigue life predictions can detect and mitigate flaw propagation before failure.

REFERENCES

6061 Aluminum: Get to Know Its Properties and Uses—Gabrian. (2020). https://www.gabrian.com/6061-aluminum-properties/

Abdalla, H. M. A., Casagrande, D., De Bona, F., De Monte, T., Sortino, M., & Totis, G. (2021). An optimized pressure vessel obtained by metal additive manufacturing: Preliminary results. *International Journal of Pressure Vessels and Piping, 192*, 104434.

Aliakbari, K., Abbasnia, S. K., & Shariati, M. (2025a). *Evaluation of the ratcheting behavior of Cr-Mo steel used in CNG tanks.*

Aliakbari, K., Abbasnia, S. K., & Shariati, M. (2025b). Evaluation of the ratcheting behavior of Cr-Mo steel used in CNG tanks. *Results in Engineering*, 104218.

Cavallo, C. (2020). *6061 Aluminum vs. 5052 Aluminum – Differences in Properties, Strength and Uses.* https://www.thomasnet.com/articles/metals-metal-products/6061-aluminum-vs-5052-aluminum/

Dean, M. (2023). *4130 Carbon Steel: Uses, Composition, Properties.* https://www.xometry.com/resources/materials/4130-carbon-steel/

Dhimole, V. K., & Cho, C. (2023, November 1). *Special Issue: Numerical Simulation and Thermo-Mechanical Investigation of Composite Structures.* EBSCOhost. https://doi.org/10.3390/app132111757

eFunda: Properties of Alloy Steel AISI 4130. (n.d.). Retrieved April 8, 2025, from https://www.efunda.com/materials/alloys/alloy_steels/show_alloy.cfm?ID=AISI_4130&Page_Title=AISI+4130&show_prop=all

Ezechukwu, V. C., Braide, T. K., Onyenanu, I. U., Ayadinuno G., Agwaziam, J. O., & Ojinekeya, C. O. (2025). Structural Simulation Analysis of the Developed Hybrid of Aluminum Composites and Carbon Nanotube Brake Disc. *International Journal of Applied and Natural Sciences, 3*(1), 18–28. https://doi.org/10.61424/ijans.v3i1.195

Ezechukwu, V. C., Oghenekaro P. O., Onyenanu, I. U., Ayadinuno, G., & Agwaziam, J. O. (2025). Mathematical Modelling and Optimization of Plantain Chip Drying: A Parametric Study on Air Frying Conditions. *IPS Journal of Engineering and Technology, 1*(1), 42–52. https://doi.org/10.54117/ijet.v1i1.13

Ezechukwu, V. C., Onyenanu, I. U., Ayadinuno, G., & Agwaziam, J. O. (2025). Structural simulation analysis of the developed hybrid of Momordica angustisepala fiber and Breadfruit seed-shell particles composites, Bolted Flanges. *IPS Journal of Engineering and Technology, 1*(1), 13–20. https://doi.org/10.54117/ijet.v1i1.2

He, J. (2023, May 30). *4130 Alloy Steel: What You Need to Know About This Versatile Alloy.* Otai Special Steel. https://www.astmsteel.com/steel-knowledge/4130-alloy-steel/

Jr, W. D. C., & Rethwisch, D. G. (2020). *Materials Science and Engineering: An Introduction.* John Wiley & Sons.

Kashyzadeh, K. R., Rahimian Koloor, S. S., Omidi Bidgoli, M., Petrů, M., & Amiri Asfarjani, A. (2021). An Optimum Fatigue Design of Polymer Composite Compressed Natural Gas Tank Using Hybrid Finite Element-Response Surface Methods. *Polymers, 13*(4), 483. https://doi.org/10.3390/polym13040483

Kim, E. S. (2019). Structural integrity evaluation of CNG pressure vessel with defects caused by heat treatment using numerical analysis. *Journal of Mechanical Science and Technology, 33*(11), 5297–5302. https://doi.org/10.1007/s12206-019-1021-7

Lee, H. (2022). *All About 4130 Steel (Properties, Strength, and Uses).* Fushun Special Steel. https://www.fushunspecialsteel.com/all-about-4130-steel-properties-strength-and-uses/

Lichtig, A. (2024). *All About 6061 Aluminum Alloy.* https://www.xometry.com/resources/materials/6061-aluminum-alloy/

Łukaszek-Sołek, A., Śleboda, T., Lisiecki, Ł., & Krawczyk, J. (2022). Hot Deformation Behavior of 4130 High-Strength Steel. *Materials, 15*(21), 7817. https://doi.org/10.3390/ma15217817

Madukasi, A. H., Onyenanu, I. U., Oghenekaro, P. O., Nzenwa, C. C., & Madu, K. E. (2025). Optimization of the Drying Parameters for Plantain Chips using a Locally Made Tray Dryer: A Study on Drying Efficiency and Drying Rate Modelling using RSM. *Journal of Food Technology & Nutrition Sciences, 7*(2), 1-10. https://doi.org/10.47363/JFTNS/2025(7)206

Omenai, S. A. (2024). *Finite Element Analysis of a Pressure Vessel Subjected to Uniform Internal Pressure.*

Onyenanu, I. U., Ofili, I., & Owuama, K. C. (2024). Eco-Friendly Brake Pad Formulation Using Agro-Waste Derived Fillers: Bush Mango Nutshell and Palm Fruit Fiber Reinforced Composites. *International Journal of Applied and Natural Sciences, 2*(2), 27–39. https://doi.org/10.61424/ijans.v2i2.152

Sharma, P., Chugh, P., & Neogi, S. (2021). Study to methodize the design of a safe Type-4 CNG storage vessel using finite element analysis with experimental validation. *International Journal of Pressure Vessels and Piping, 192*, 104425. https://doi.org/10.1016/j.ijpvp.2021.104425

Soo Kim, E. (2019). Evaluation of Rupture Characteristics of CNG Vehicle Container by Heat Treatment using AUTODYN. *IOP Conference Series: Materials Science and Engineering, 673*(1), 012107. https://doi.org/10.1088/1757-899X/673/1/012107

Team, G. (2018). *6061 Aluminum: Get to Know Its Properties and Uses.* Gabrian. https://www.gabrian.com/6061-aluminum-properties/

Thamaraiselvi, K., & Vishnuvardhan, S. (2020). Fracture studies on reactor pressure vessel subjected to pressurised thermal shock: A review. *Nuclear Engineering and Design, 360*, 110471. https://doi.org/10.1016/j.nucengdes.2019.110471

Toudehdehghan, A., & Hong, T. W. (2019). A critical review and analysis of pressure vessel structures. *IOP Conference Series: Materials Science and Engineering, 469*(1), 012009. https://doi.org/10.1088/1757-899X/469/1/012009

Tsonos, A. (2017). *Structural design of CNG storing composite pressure vessels for marine applications.* https://dspace.lib.ntua.gr/xmlui/bitstream/handle/123456789/46054/Tsonos_Angelos_Thesis.pdf?sequence=1

Willden, C., & Jensen, W. A. (2020). Optimal designs with axial values. *Journal of Quality Technology, 52*(3), 235-248. https://www.tandfonline.com/doi/abs/10.1080/00224065.2019.1571346